

Flow features induced by a rod-shaped microswimmer and its swimming efficiency: A two-dimensional numerical study

Siwen Li(李斯文), Yuxiang Ying(应宇翔), Tongxiao Jiang(姜童晓), and Deming Nie(聂德明)

Citation: Chin. Phys. B, 2024, 33 (**12**): 124701. DOI: 10.1088/1674-1056/ad84c3
Journal homepage: http://cpb.iphy.ac.cn; http://iopscience.iop.org/cpb

What follows is a list of articles you may be interested in

Effect of local wall temperature on hypersonic boundary layer stability and transition

Ruiyang Lu(鲁锐洋) and Zhangfeng Huang(黄章峰)
Chin. Phys. B, 2023, 32 (**11**): 114701. DOI: 10.1088/1674-1056/acea69

Characteristics of temperature fluctuation in two-dimensional turbulent Rayleigh-Bénard convection

Ming-Wei Fang(方明卫), Jian-Chao He(何建超), Zhan-Chao Hu(胡战超), and Yun Bao(包芸)
Chin. Phys. B, 2022, 31 (**1**): 014701. DOI: 10.1088/1674-1056/ac012f

Effects of Prandtl number in two-dimensional turbulent convection

Jian-Chao He(何建超), Ming-Wei Fang(方明卫), Zhen-Yuan Gao(高振源), Shi-Di Huang(黄仕迪), and Yun Bao(包芸)
Chin. Phys. B, 2021, 30 (**9**): 094701. DOI: 10.1088/1674-1056/ac0781

Characteristics and generation of elastic turbulence in a three-dimensional parallel plate channel using direct numerical simulation

Hong-Na Zhang(张红娜), Feng-Chen Li(李凤臣), Xiao-Bin Li(李小斌), Dong-Yang Li(李东阳), Wei-Hua Cai(蔡伟华), Bo Yu(宇波)
Chin. Phys. B, 2016, 25 (**9**): 094701. DOI: 10.1088/1674-1056/25/9/094701

Effects of the computational domain on the secondary flow in turbulent plane Couette flow

Gai Jie (盖杰), Xia Zhen-Hua (夏振华), Cai Qing-Dong (蔡庆东)
Chin. Phys. B, 2015, 24 (**10**): 104701. DOI: 10.1088/1674-1056/24/10/104701

Flow features induced by a rod-shaped microswimmer and its swimming efficiency: A two-dimensional numerical study

Siwen Li(李斯文)[1], Yuxiang Ying(应宇翔)[2], Tongxiao Jiang(姜童晓)[1], and Deming Nie(聂德明)[1,†]

[1] *College of Metrology Measurement and Instrument, China Jiliang University, Hangzhou* 310018, *China*
[2] *Institute of Fluid Engineering, Zhejiang University, Hangzhou* 310018, *China*

(Received 9 July 2024; revised manuscript received 10 September 2024; accepted manuscript online 9 October 2024)

The swimming performance of rod-shaped microswimmers in a channel was numerically investigated using the two-dimensional lattice Boltzmann method (LBM). We considered variable-length squirmer rods, assembled from circular squirmer models with self-propulsion mechanisms, and analyzed the effects of the Reynolds number (Re), aspect ratio (ε), squirmer-type factor (β) and blockage ratio (κ) on swimming efficiency (η) and power expenditure (P). The results show no significant difference in power expenditure between pushers (microswimmers propelled from the tail) and pullers (microswimmers propelled from the head) at the low Reynolds numbers adopted in this study. However, the swimming efficiency of pushers surpasses that of pullers. Moreover, as the degree of channel blockage increases (i.e., κ increases), the squirmer rod consumes more energy while swimming, and its swimming efficiency also increases, which is clearly reflected when $\varepsilon \leq 3$. Notably, squirmer rods with a larger aspect ratio ε and a β value approaching 0 can achieve high swimming efficiency with lower power expenditure. The advantages of self-propelled microswimmers are manifested when $\varepsilon > 4$ and $\beta = \pm 1$, where the squirmer rod consumes less energy than a passive rod driven by an external field. These findings underscore the potential for designing more efficient microswimmers by carefully considering the interactions between the microswimmer geometry, propulsion mechanism and fluid dynamic environment.

Keywords: direct numerical simulations, low-Reynolds-number motions, multiphase flows, swimming microorganisms

PACS: 47.27.ek, 47.63.mf, 47.61.Jd, 47.63.Gd **DOI:** 10.1088/1674-1056/ad84c3

1. Introduction

As an emerging field of robotics, microrobots that navigate and swim in viscous fluids offer tremendous potential in the biomedical domain, including applications in minimally invasive surgery, targeted drug delivery, immunotherapy and detoxification.[1–4] To design microswimmers in an ideal swimming state, researchers are often inspired by nature (such as fish, jellyfish and snakes[5–7]). Considering the special environment and operational requirements inside the human body, such as the high-viscosity fluid environment of blood, microbial-inspired robots have a more efficient way of moving. Utilizing viscous forces to propel forward, reduce resistance, and more easily pass through blood vessels and certain media to reach the target area is an ideal choice for medical applications.

In low-Reynolds-number (low-Re) fluid environments, some bacteria can move tens or even hundreds of times their own length per second and maintain the stability of their motions. They have superior motility in microscale environments compared to macroscopic conditions, due to their propulsive structures: flagellums and cilia — currently mimicked by many microrobots as their drive motors, such as the magnetic helical microrobot inspired by the motion of E. coli's caudal flagellum[8] and the artificial bacterial flagellum (ABF), often used in the study of microswimmers in low-Re environments. Gong *et al.*[9] utilized nickel-plated spirulina to create bioinspired magnetic helical microswimmers that could be flexibly propelled and steered in deionized water at an enhanced propulsion speed. Self-folding helical microrobots improved drug release efficiency under ultrasonic stimulation.[10] In addition, considering the exclusivity of the human immune system, biohybrid microswimmers are emerging. Compared with traditional mechanical devices, these microswimmers possess biocompatibility and detectability, enabling them to complete tasks more effectively. Akolpoglu *et al.*[11] studied biohybrid microalgae that delivered chemotherapeutic drugs to tumor cells by embedding them in a nano coating on the surface of chlamydomonas. Alapan *et al.*[12] used escherichia coli to drive erythrocytes with anticancer drugs through micrometer channels. Veronika *et al.*[13] mimicked sperm motile cell motility to fabricate a microswimmer with a magnetic field controlling the non-motile sperm flagellum to maintain its locomotor agility for rapid targeted drug delivery at a specific frequency.

The squirmer model,[14] a pivotal contribution by Lighthill and later expanded by Blake, offers a comprehensive physical and mathematical framework for understanding the propulsion strategies of microorganisms such as bacteria, lacewings and algae. This model intricately describes how these microorganisms navigate through fluid environments by

†Corresponding author. E-mail: nieinhz@cjlu.edu.cn

© 2024 Chinese Physical Society and IOP Publishing Ltd

leveraging surface structures, notably flagella and cilia, for propulsion. For simplification, the squirmer model introduces a prescribed slip-velocity formula on its surface, which encapsulates the essence of microorganism propulsion. Within this framework, two distinct propulsion mechanisms emerge: pusher and puller. The pusher mechanism, exemplified by the tail-driven propulsion of E. coli, highlights how some microorganisms generate forward movements by pushing the fluid behind them. Conversely, the puller mechanism, as demonstrated by the head-driven propulsion of chlamydomonas, illustrates the forward thrust generated by pulling the fluid towards the organism. The versatility of the squirmer model has made it an indispensable tool for exploring microbial motility and designing microswimmers. It is widely used to study microbial motility or microswimmers,[15] including nutrient uptake,[16,17] collective behavior,[18–20] settling motility[21,22] and wall action.[23,24] The study of microbial motility mechanisms is fundamental for the development of both artificial swimming devices and biohybrid microswimmers, bridging the gap between synthetic engineering and biological functionalities.

In the process of developing bionic microrobots, improving the swimming efficiency with limited energy input has become a popular research topic. Gioia *et al.*[25] proposed an energy-efficient propulsion method for magnetic gradient traction microrobots that consumes only one-ninth of the power of the original method while achieving the same accuracy and speed, thereby reducing energy consumption. Acemoglu *et al.*[26] simulated the motion of helical flagellar microswimmers in microchannels and analyzed the effects of helical radius, channel radius, etc, on swimming speed and efficiency, with the results indicating that for thick flagellums with increasing caudal radius, a critical channel radius exists that maximizes the speed and efficiency of the swimmer. Franziska *et al.*[27] investigated the effect of collagen concentration on the propulsive speed of spiral microswimmers and proposed a relationship between magnetic field strength, swimming speed and efficiency. Ali *et al.*[28] designed a ciliated microswimming robot with a maximum speed of 45 mm/s and an efficiency of 40%. Toshihiro *et al.*[29] showed that ciliates can increase their self-propulsion efficiency up to 100 times by increasing the number of cilia.

Regarding the squirmer model, in agreement with the definitions proposed by many studies,[30–32] swimming efficiency is usually defined as the ratio of the power of the two modes of motion (passive rigid body motion driven by external forces and self-propelled motion). Chisholm *et al.*[33] investigated the flow field around a squirmer with *Re* ranging from 0.1 to 1000 and showed that the velocity of the pusher increases monotonically with the *Re*, the pusher swam more efficiently and the flow field around it was more stable compared to that of the pusher at larger *Re*. Similar conclusions were drawn by Ouyang *et al.*[30] who numerically studied the motion of a squirmer in a power-law fluid with a low *Re*. The velocity of a squirmer in a shear-thin fluid is slower than that in a Newtonian fluid, the hydrodynamic efficiency of a pusher in the same type of fluid monotonically increases with an increase in *Re* and that of a pusher shows non-monotonicity. Patrick *et al.*[34] investigated the motion of a squirmer in a fluid whose viscosity varied with temperature, assuming that the fluid had a constant viscosity and that more energy was required to achieve the envisioned speeds because the power consumption of actual biological swimmers was much greater than that calculated by the model. In viscoelastic fluids, increasing fluid elasticity leads to a reduction in energy consumption and an increase in swimming efficiency, and a gait with vortices is less efficient than that without vortices.[35] Ardekani *et al.*[36] showed that, in the inertial state, the pusher has better competitive performance, swimming speed and swimming efficiency than the puller. Considering the effect of the wall surface, Zhu *et al.*[37] investigated swimming in capillary tubes and showed that near-wall motion always increased the energy consumption of swimmers with either tangential or normal surface deformations. Considering the ability to transport cargo, Ouyang *et al.*[38] numerically investigated microswimmers carrying rigid objects and proposed four carrying modes, among which the pusher-cargo model had the highest swimming speed, the cargo-pusher model had the maximum swimming efficiency, and the puller-cargo model was more stable than the cargo-puller model.

However, both natural bacteria and swimmers in medical applications tend not to be perfectly spherical, and most of the previously mentioned swimming devices are characterized by elongation, with non-spherical bacteria bots having a high aspect ratio of the body having greater directionality than non-spherical ones with a low aspect ratio.[39] Compared to spheres, elongated or rod-shaped particles have a longer circulation time in the blood[40,41] making them more likely to accumulate at the site of the lesion[42] and less filtered in the liver, thus reducing the risk of renal disease, which is of great significance for drug delivery. Ying *et al.*[43] investigated the settling behavior of an elliptical squirmer in the channel. In contrast to the circular squirmer, the head direction of the elliptical squirmer tends to follow the direction of the fluid flow to reduce its own drag force. Zantop and Stark[44] arranged several spherical squirmers on a line and analyzed the flow field of squirmer rods with different plate widths using the mesoscale simulation method of multiparticle collision dynamics because the rods generate extra torque resulting in a more complex flow field for the lengthy. For the long pusher and puller, the flow field consists of four hydrodynamic moments: a force dipole, source dipole, force quadrupole and

source octupole. For the pusher-like squirmer rod with a significant elongation consisting of four hydrodynamic moments, the force dipole completely dominates the flow field, and its predominance is dependent on the plate width and radial distance. Similarly, using the immersed boundary-lattice Boltzmann method (IB-LBM), Ouyang *et al.*[45] combined several squirmers in tandem to form a squirmer rod and investigated the effects of the *Re*, number of squirters and squirter spacing on the swimming performance of the microswimmer. The effect of squirmer spacing on the swimming performance of microswimmers showed that at $Re < 0.1$, the speed of the squirmer rod increased with an increase in the number of squirmers due to the dominance of viscous forces — not related to the type of swimming. When $Re > 1$, the power consumed by the pusher and puller increases monotonically, and a smaller number of combinations and larger spacing are more favorable for swimming efficiency. Moreover, Takuji *et al.*[46] proposed two types of dumbbells that connect two squirmers with a rigid rod: side-by-side, fore, and aft. Using the puller as the fore squirmer and the pusher as the aft squirmer increased the swimming speed of the squirmer. When the puller acts as a fore squirmer and the pusher as an aft squirmer, the swimming speed is substantially increased.

Swimming efficiency is a focus in the design of microrobots for future engineering applications. Despite the extensive studies on squirmer motion in the past, there has been more emphasis on velocity, locomotive modes and flow field variations, with little focused discussion on swimming efficiency or consideration of single factors. Therefore, we conducted a comprehensive analysis from multiple perspectives of the microswimmer itself (the aspect ratio and the squirmer-type factor) and the external environment (Reynolds number and the blockage ratio) in this study. On the one hand, most studies are still confined to circular or spherical squirmers. However, real microorganism shapes tend to have elongated bodies and do not have raised surfaces. Therefore, we constructed a squirmer rod with a smooth body surface closer in shape to real microorganisms, such as E. coli. We represented the variation in size based on the aspect ratio rather than the number and spacing of circles, which can greatly simplify the selection of parameters and the presentation of results. On the other hand, the influence of the channel wall is not considered, and in some studies microswimmers only swim freely in an unlimited flow field. Biondi *et al.*[47] reported that E. coli decreases its velocity due to drag effects in channels sized close to it and Zhang *et al.*[48] indicated that confinement to pipe-like constraints can enhance or hinder the speed of microswimmers. Thus, the blockage ratio is an important factor for the study of swimming performance. In addition, considering the development prospect of microswimmers, according to the definition of efficiency, we evaluated the energy consumption of the two modes of movement under different factors, which were not mentioned in previous studies. We hope that the results and discussions of this work can provide help with the selection and design of bionic micro-robots in the future.

In Section 2, we present the LBM, squirmer rod model and treatment of the boundary conditions as well as the formulas for swimming efficiency and power expenditure of the swimmer. Section 3 presents the computational model and parameters. The results of the effects of the *Re*, length-to-diameter ratio (ε), squirmer-type factor (β) and blockage ratio (κ) on swimming efficiency (η) as well as power expenditure (P) are shown in Section 4, respectively. Finally, a summary of the results is presented in Section 5.

2. Numerical method

2.1. Lattice Boltzmann method

The lattice Boltzmann method (LBM) transforms the fluid flow problem in a continuum into the particle motion problem in a discrete space and realizes the exchange of momentum and energy through the streaming and collision of particles.[49] The evolution of the distribution function of each lattice node is calculated to obtain the macroscopic information of the flow field. The complete LBM usually consists of three parts:[50] discrete velocity model, equilibrium distribution function and evolution equation of distribution function. We selected the D2Q9 model proposed by Qian *et al.*[51] The microscopic velocity $\boldsymbol{e}_i$ is shown in Fig. 1, and c is the lattice velocity, $c = \Delta x/\Delta t$, where Δx is the lattice grid and Δt is the time step of the simulation. For simplicity, Δx and Δt are both set at 1 in this paper.

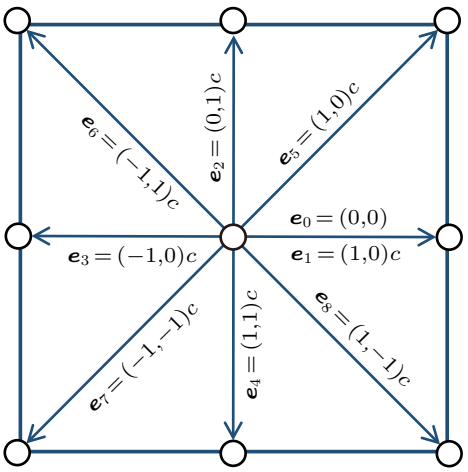


Fig. 1. The D2Q9 model (nine discrete velocities in two dimensions).

The particles on each lattice node correspond to the density distribution function $f_i(\boldsymbol{x},t)$, and the density ρ and velocity $\boldsymbol{u}$ of a fluid on the macroscopic scale can be obtained using the following equations:

$$\rho = \sum_i f_i, \quad \rho \boldsymbol{u} = \sum_i f_i \boldsymbol{e}_i. \tag{1}$$

The equilibrium distribution function determined by the D2Q9 model is expressed as

$$f_i^{(\mathrm{eq})} = w_i \rho \left[1 + \frac{\boldsymbol{e}_i \cdot \boldsymbol{u}}{c_\mathrm{s}^2} + \frac{(\boldsymbol{e}_i \cdot \boldsymbol{u})^2}{2c_\mathrm{s}^4} - \frac{\boldsymbol{u}^2}{2c_\mathrm{s}^2} \right], \tag{2}$$

where w_i denotes a weight factor of 4/9, 1/9, 1/9, 1/9, 1/9, 1/36, 1/36, 1/36 and 1/36, corresponding to i from 0 to 8. c_s is the speed of sound and $c_\mathrm{s} = c/\sqrt{3}$. The discrete lattice Boltzmann equations are

$$\begin{aligned} & f_i(\boldsymbol{x} + \boldsymbol{e}_i \Delta t, t + \Delta t) - f_i(\boldsymbol{x}, t) \\ = & -\frac{1}{\tau} \left[f_i(\boldsymbol{x}, t) - f_i^{(\mathrm{eq})}(\boldsymbol{x}, t) \right], \end{aligned} \tag{3}$$

where τ is the relaxation time, and the motion of particles is divided into streaming (left term of Eq. (3)) and collision (right term of Eq. (3)), which is an important characteristic of LBM. The macroscopic mass and momentum equations in the low Mach number limit are obtained by the Chapman–Enskog[52] expansion as follows:

$$\frac{\partial \rho}{\partial t} + \nabla \cdot (\rho \boldsymbol{u}) = 0, \tag{4}$$

$$\frac{\partial (\rho \boldsymbol{u})}{\partial t} + \nabla \cdot (\rho \boldsymbol{u}\boldsymbol{u}) = -\boldsymbol{\nabla} p + \rho \nu \nabla^2 \boldsymbol{u}. \tag{5}$$

In this paper, the kinematic viscosity of the fluid is related to the relaxation time, as explicitly defined by the formula $\nu = c_\mathrm{s}^2(\tau - 0.5)\Delta t$.

2.2. Squirmer rod model

In this study, the squirmer model proposed by Blake[14] is adopted as the basic element for assembling the squirmer rods. This model assumes a wave envelope on the surface of the microswimmer to simulate the oscillation of the microbial ciliary population. The two-dimensional squirmer model surface imposes the prescribed radial and tangential velocity components as follows:

$$\boldsymbol{u}^\mathrm{s}(\boldsymbol{r}) = \sum_{n=0}^{\infty} A_n \cos(n\theta)\hat{\boldsymbol{r}} + \sum_{n=1}^{\infty} B_n \sin(n\theta)\hat{\boldsymbol{\theta}}, \tag{6}$$

where $\hat{\boldsymbol{\theta}}$ and $\hat{\boldsymbol{r}}$ denote the polar and radial unit vectors, respectively, at the point on the boundary of the squirmer model. A_n and B_n are the corresponding time-dependent amplitudes. When studying the motion of a squirmer, researchers tend to neglect radial deformation and simplify the model using the tangential slip velocity

$$u^\mathrm{s}(\theta) = (B_1 \sin\theta + 2B_2 \sin\theta \cos\theta)\hat{\boldsymbol{\theta}}. \tag{7}$$

The term with coefficient B_1 in Eq. (7) primarily drives the propulsion of the squirmer, leading to a stable swimming speed of $B_1/2$ for a squirmer in a Stokes flow. The term with coefficient B_2 induces vortices around the squirmer. Figure 2 shows a schematic of the squirmer rod comprising the squirmer model. We select several circular squirmers arranged in series at equal intervals (we provide four squirmers as an example in the figure), where l is the rod length, d is the diameter, and s represents the distance between the centers of mass of two neighboring squirmers. The velocity at the intersecting parts of the adjacent circles (indicated by dashed lines) is set at 0 to ensure that the tangential velocity exists only at the shape boundary. Squirmer rods with different aspect ratios ε are composed of varying numbers of circles and spacing.

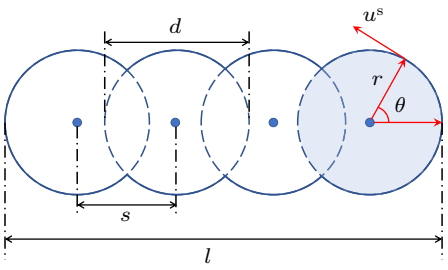


Fig. 2. Schematic diagram of the squirmer rod model.

The type of swimming is categorized into three types according to the parameter $\beta = B_2/B_1$: pusher ($\beta < 0$), puller ($\beta > 0$) and neutral squirmer ($\beta = 0$). Figure 3 shows the distribution of velocity vectors for the three swimming types of the squirmer rod, with the purple squirmer rod representing the pusher, the yellow rod representing the neutral, the green rod representing the puller, and the arrow on the axis pointing to the head. Notably, the direction of velocity on both sides of the body of the squirmer rod is directed from the head to the tail, with the main difference being at the ends. This study focuses on the first two types of squirmer motion. A pusher is a type of microswimmer (such as E. coli and sperm) that propels itself by pushing fluid with its tail cilia, obtaining thrust for navigation. Conversely, a puller draws fluid towards its body with cilia located at the head, generating propulsion (as observed in organisms such as chlamydomonas). Although the neutral squirmer rod is not the main subject of this study, as a contrast it can be seen that its surface velocity was smaller than that of the other two types. In addition, its self-propelled velocity distribution was relatively uniform, with no dominant component exhibiting strong propulsion.

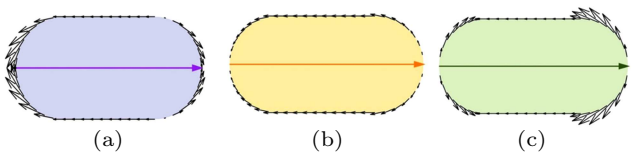


Fig. 3. Schematic diagram of the squirmer rod boundary tangential velocity vector, with the scale factor of the arrow defined as λ: (a) pusher ($\beta = -3$, $\lambda = 0.8$), (b) neutral squirmer rod ($\beta = 0$, $\lambda = 1.2$) and (c) puller ($\beta = 3$, $\lambda = 0.8$).

2.3. Boundary conditions

In the simulations using the LBM, to implement a no-slip boundary condition on the squirmer surface, we adopted an improved bounce-back scheme with second-order accuracy, as proposed by Lallemand and Luo.[53] As depicted in Fig. 4, the hollow circles represent fluid nodes, and gray triangles denote solid nodes. The light blue circle and the dark blue circle represent the solid particle at the previous and next moment, respectively. Note that some nodes change during the movement of the solid particle, the original fluid nodes transform into covered fluid nodes (solid nodes), represented by green triangles, and the original solid nodes transform into uncovered fluid nodes, represented by white triangles. Taking fluid node A as an example, the distribution function f_6 that should be passed from node S to node A needs to be recalculated according to the interpolation scheme because of the movement of the solid boundary, which depends on the exact position of the boundary node P. Therefore, a parameter $q = |AP|/|AS|$ is introduced in the scheme to represent the volume fraction of the fluid region, and the update of f_6 based on the value of q is calculated as follows:

$$f_6(A) = \begin{cases} q(1+2q)f_8(S) + (1-4q^2)f_8(A) - q(1-2q)f_8(B) - 2w_8\rho_f \dfrac{\boldsymbol{e}_8 \cdot \boldsymbol{u}_P}{c_s^2}, & q < \dfrac{1}{2}, \\ \dfrac{1}{q(2q+1)}f_8(S) + \dfrac{2q-1}{q}f_6(B) - \dfrac{2q-1}{2q+1}f_6(C) - \dfrac{2w_8\rho_f}{q(2q+1)}\dfrac{\boldsymbol{e}_8 \cdot \boldsymbol{u}_P}{c_s^2}, & q \geq \dfrac{1}{2}, \end{cases} \tag{8}$$

where $\boldsymbol{u}_P$ is the velocity of node P, including the self-propelled velocity of the squirmer rod in this study. More details about the improved bounce scheme can be found in the literature.

A scan is performed on the boundary nodes encircling the surface of the squirmer, with the momentum exchange technique[54,55] employed to determine the forces and torques exerted on each boundary node. As the squirmer moved, the fluid and solid nodes interchanged because of the change in the position of the squirmer. Hence, considering these changing nodes, we employ the method proposed by Aidun *et al.*[55] to calculate additional forces and torques, and the motion of the squirmer is solved using Newton's equations by calculating the complete forces and moments.

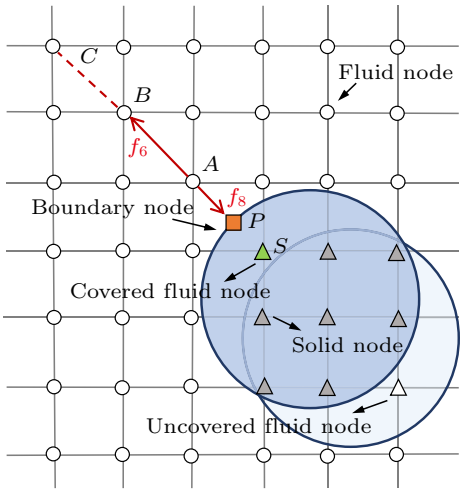


Fig. 4. Schematic diagram of the improved bounce-back scheme.[53]

2.4. Swimming power and hydrodynamic efficiency

In Newtonian Stokes flow, the swimming power expenditure of a two-dimensional squirmer rod with only tangential velocity can be calculated as follows:

$$P = -\int_s \boldsymbol{n}\cdot\boldsymbol{\sigma}\cdot(\boldsymbol{U}+\boldsymbol{u}_{\boldsymbol{\theta}})\,\mathrm{d}S, \tag{9}$$

where $\boldsymbol{n}$ is the outward unit normal vector of the squirmer rod's surface, $\boldsymbol{\sigma}$ is the fluid's stress tensor, and $\boldsymbol{U}$ and $\boldsymbol{u}_{\boldsymbol{\theta}}$ are the translational and tangential velocities of the squirmer rod, respectively.

The hydrodynamic efficiency of a swimmer at low *Re* values is often defined as

$$\eta = \frac{\boldsymbol{F}\cdot\boldsymbol{U}_{\mathrm{g}}}{P}, \tag{10}$$

where $\boldsymbol{F}$ represents the force required to drag a passive rigid body of the same shape as the microswimmer to achieve the microswimmer's steady velocity $\boldsymbol{U}_{\mathrm{g}}$ and P is the rate of power dissipation during swimming. In real natural environments, the energy consumption of microorganisms includes complex activities such as metabolism, and in this study, we consider the swimming efficiency only in terms of hydrodynamics, which can be interpreted as a relative measure of the power dissipated by viscous stresses while the microswimmer is moving in the fluid, and therefore does not have to be less than one.[56]

3. Problem description

As shown in Fig. 5, we simulated the motion of a squirmer rod in a horizontal channel filled with stationary fluid and calculated its power expenditure and swimming efficiency. The length and width of the channel were $L = 40d$ and $H = 8d$, respectively, and the top and bottom sides were set as walls with no-slip boundary conditions. The upstream was set as undisturbed, and the downstream was set as fully developed boundary conditions. In the study of the aspect ratio of the

squirmer rod within this paper, to ensure that the model always maintains the same distance from the walls on both sides, the diameter d is fixed at $40\Delta x$, and only its length l is varied from $40\Delta x$ to $240\Delta x$ to change the aspect ratio $\varepsilon = l/d$ from 1 to 6. The channel's width is adjusted to ensure that the channel blockage ratio $\kappa = d/H$ varies from 0.083 to 0.25. The swimming Re is defined as $Re = U_s d/\nu$. To ensure sufficient movement time for the fish to swim at a steady velocity, we used a moving mesh to ensure it was always located in the center of the horizontal channel.

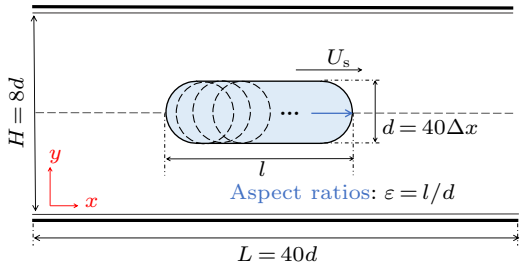


Fig. 5. Schematic diagram of the calculation model.

4. Results

In this section, we present the results of the simulations and discuss the effect of Re, the aspect ratio (ε), the squirmer-type factor (β) and the blockage ratio (κ) on the swimming efficiency of the squirmer rod as well as on the power expenditure in four subsections. In each subsection, we present graphs illustrating the relationship between swimming efficiency and the corresponding parameters. We mainly explain the reasons for the changes in swimming efficiency during the motion of the squirmer rod from the perspective of power consumption, and the pressure distribution of the flow field and the streamline structure are also provided. Note that the squirmer rod with $\varepsilon = 1$ is seen as a circular squirmer, the purple squirmer rod in all flow field diagrams represents a pusher, and the green rod represents a puller. Unless specifically mentioned, the blockage ratio (κ) is set at 0.125.

4.1. Effects of the Reynolds number

Figure 6(a) shows the variation in swimming efficiency for pushers ($\beta = -3$) and pullers ($\beta = 3$) across three aspect ratios ($\varepsilon = 1$, 2 and 3) as Re ranges from 0.005 to 0.5. The results indicate that, for both circular squirmers and squirmer rods with varying aspect ratios, as the Re increases, the swimming efficiency (η) of pushers shows a monotonically increasing trend, whereas that of pullers shows a declining trend, clearly reflected at $Re > 0.1$. At a lower Re, there is no significant difference in swimming efficiency between the two groups. Figure 6(b) depicts the variation in swimming power (P) and steady swimming speed (U) for the same conditions as in Fig. 6(a), where P and U have been normalized, and the results for $\varepsilon = 3$ are given here for illustration purposes. The difference in swimming efficiency between pushers and pullers mainly stems from the differences in their respective swimming speeds. Although microswimmers move in Stokes flow, the lower inertia cannot be neglected when Re increases to a certain value, which leads to an increase in the pusher's velocity and a suppression of the puller's velocity, similar to many research findings on the squirmer model.[33,36] When Re decreases to the point where inertia can be ignored, the swimming types have little effect on the swimming efficiency.

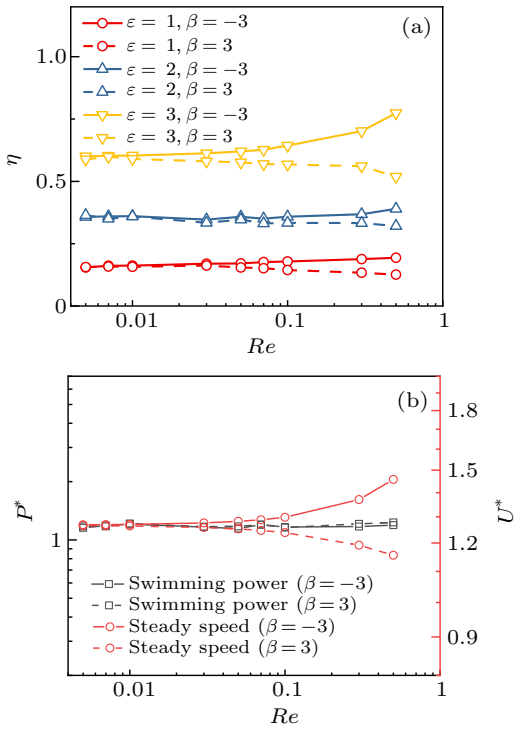


Fig. 6. Function of Re for different types ($\beta = \pm 3$). (a) Swimming efficiency for $\varepsilon = 1$, 2, 3. (b) Power expenditure and steady velocity for $\varepsilon = 3$ (P and U are normalized by $B_1^2 \mu d/4$ and $B_1/2$, respectively).

A comparison of the flow fields of the two swimming types at $Re = 0.005$ (top) and $Re = 0.5$ (bottom) is shown in Fig. 7. Because of the axisymmetric distribution of the flow structure around the squirmer rod, for ease of observation, we show the flow structure on only one side, with the black flow line representing $Re = 0.005$ and the red flow line representing $Re = 0.5$. In the fluid dynamics analysis of the pushers and pullers, a notable phenomenon is the distinct distribution of the pressure areas. For pushers, the high-pressure areas formed at the front and rear along with the low-pressure areas at the sides constitute their unique fluid-dynamic characteristics. This structure enables the pushers to effectively draw fluid from the sides and expel it through the front and rear sides. Conversely, the pullers display a different pattern of fluid interaction, with low-pressure areas at the front and rear and high-pressure areas on the sides. By drawing fluid towards themselves from the front and rear, and then expelling it from the sides, pullers contrast sharply with pushers in terms of their

propulsion mechanisms. Furthermore, flow field analysis reveals that the recirculation zones upstream of both the pushers and pullers are effectively suppressed, whereas the downstream recirculation zones are significantly expanded. This adjustment in the flow field provides pushers with a stronger propulsion force because they can more effectively use the thrust generated at their tails to move through the fluid. In contrast, pullers that rely on head-driven propulsion experience a reduction in thrust and, as a result, a decrease in speed. Even in Stokes flow, which is dominated by viscous forces, a slight increase in inertial forces can significantly affect the speeds of these two types of microswimmers, leading to an increase in the speed of the pushers and a decrease in the speed of the pullers. As mentioned in the definition of swimming efficiency in Subsection 2.4, dragging a passive rigid body requires the same stabilizing speed as a squirmer rod. Thus, achieving a higher speed requires a stronger external force and consumes more energy. In contrast to passive particles, the self-propelling squirmer rod does not display such a relationship, and the variance in swimming speeds between the pushers and pullers does not affect their power expenditure during movement. Therefore, at low Re values ($Re < 0.1$), the swimming efficiencies of the pushers and pullers are similar, making either swimming type a viable option. When the Re is slightly higher ($0.1 < Re \leq 0.5$), higher swimming efficiency can be achieved by choosing pushers. Furthermore, we observe that elongating the body of the squirmer rod affects its swimming performance, which will be detailed in the following section.

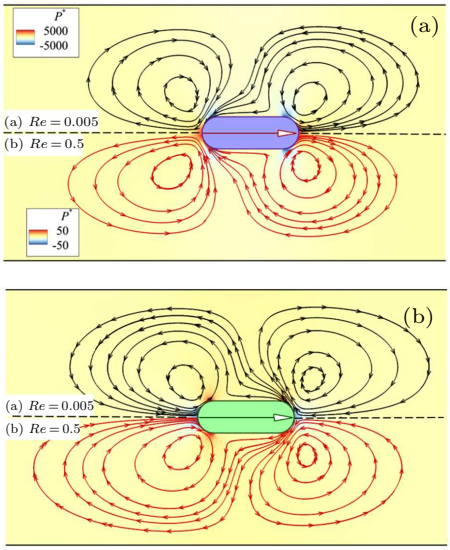


Fig. 7. Streamlines around a squirmer rod at $Re = 0.005$ and $Re = 0.5$ for $\varepsilon = 3$. (a) Pusher ($\beta = -3$) and (b) puller ($\beta = 3$).

4.2. Effects of the aspect ratios

Body length often has a key influence on the swimming performance of microswimmers. Microorganisms in nature utilize elongated bodies to adapt to various fluid environments and ensure optimal swimming conditions. For $Re = 0.005$, 0.05 and 0.5, the results for pusher ($\beta = -3$) and puller ($\beta = 3$) after increasing the length of the body are consistent with that described in the previous section. Hence, we conduct our analysis for the case of $Re = 0.005$. As illustrated in Fig. 8(a), the swimming efficiency of the squirmer rod exhibits a nonlinear monotonically increasing relationship with increasing ε in both swimming types. From the velocity vector distribution of the squirmer rod shown in Fig. 3, an increase in the aspect ratio results in a wider distribution of self-propelled velocities on both sides of the body but does not affect the circular head and tail ends, which can be visualized as more cilia to aid swimming in long strip-shaped microorganisms. Squirmer rods with larger aspect ratios exhibit higher self-propelled swimming speeds, suggesting that more energy is expended to drag a correspondingly longer passive rigid body, as indicated by the change in FU_g in Fig. 8(b). This consideration is critical when studying how microswimmers move through fluids, particularly when focusing on improving energy efficiency and enhancing propulsion. Interestingly, the data shown in Fig. 8(b) suggest that the power expenditure of the self-propelled squirmer rod decreased as ε increased, implying that, although the volume and surface area of the squirmer rod increase with the aspect ratio, they achieve more efficient movement in fluids by optimizing their shape and propulsion methods, thereby reducing the overall energy requirement.

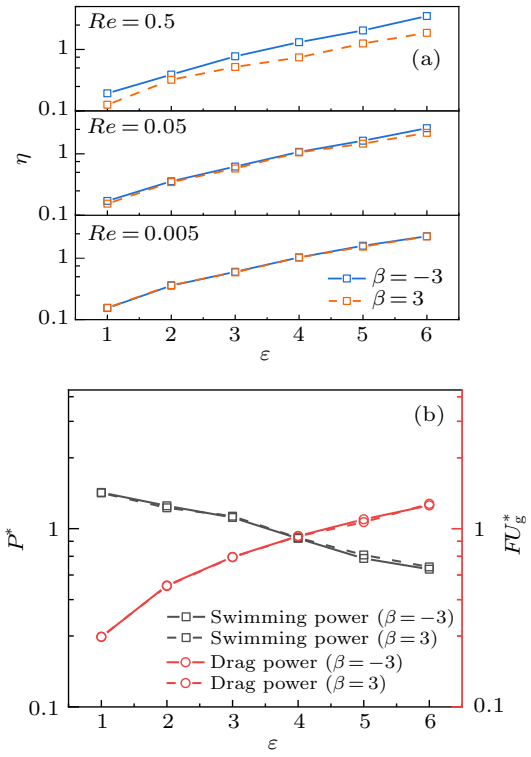


Fig. 8. Function of aspect ratios (ε). (a) Swimming efficiency for $Re = 0.005$, 0.05 and 0.5. (b) Power expenditure for $Re = 0.005$ (P and FU_g are normalized by $B_1^2 \mu d/4$).

We selected squirmer rods with aspect ratios of $\varepsilon = 2$, 4 and 6 to show their flow field in Fig. 9. Within a channel of limited width, changes in the recirculation zones around the squirmer rod can be observed, influenced by the aspect ratio. For example, at $\varepsilon = 2$, the fluid is quickly attracted by the low-pressure area at the tail after being impacted by the high-pressure area at the head, resulting in four compact recirculation zones. When $\varepsilon = 4$, there is no significant change in the pair of symmetrical recirculation zones at the tail of the pusher and head of the puller. However, the recirculation zones close to the head of the pusher and tail of the puller are noticeably stretched. The path of the fluid flowing from the head to the tail is extended, making it easier for the fluid to flow close to the surface of the squirmer rod, thereby reducing the fluid resistance encountered during swimming. This effect is even more pronounced at $\varepsilon = 6$. In addition, in environments with high-viscosity fluids, elongated squirmer rods can harness these recirculation zones more efficiently for additional propulsion, thereby consuming less energy, consistent with the locomotion patterns observed in natural microorganisms. Some bacteria and algae tend to utilize their long, slender bodies to sense the fluid environment and adjust their movement over time to absorb nutrients more efficiently.

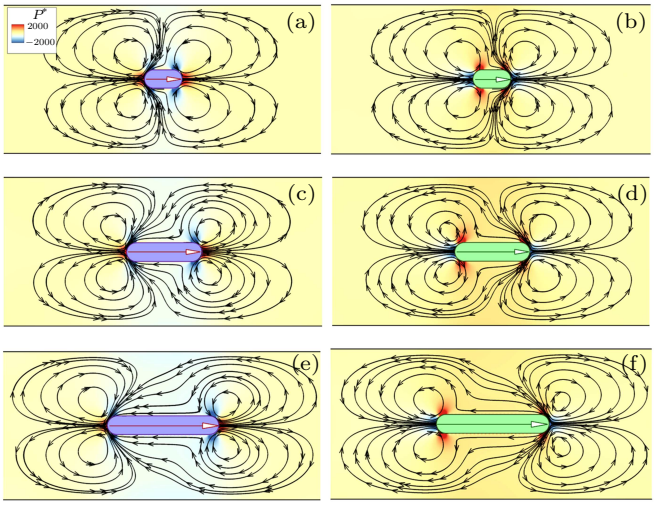


Fig. 9. Streamlines around a squirmer rod at $Re = 0.005$. (a) $\varepsilon = 2$, $\beta = -3$, (b) $\varepsilon = 2$, $\beta = 3$, (c) $\varepsilon = 4$, $\beta = -3$, (d) $\varepsilon = 4$, $\beta = 3$, (e) $\varepsilon = 6$, $\beta = -3$ and (f) $\varepsilon = 6$, $\beta = 3$.

For the squirmer rods simulated in this study, a longer body reduces energy consumption and enhances swimming efficiency, representing the ideal goal for designing numerous microswimming devices. However, this aspect also requires consideration of actual application scenarios, making the appropriate selection of the microswimmer's aspect ratio crucial. Moreover, we notice that the drag and swimming powers are almost equal numerically when ε is 4, which means that moving at the same speed, a squirmer rod can consume approximately the same power as driving a passive rod using an external field. However, if we want to accomplish the target task with a rod microswimmer with an aspect ratio greater than 4, using an external field driver may not be appropriate since it requires a relatively large amount of power expenditure.

4.3. Effects of the squirmer type

In the previous discussions, we introduced two swimming strategies for the squirmer rod: pusher and puller, both influenced by the sign of β. To examine the implications of changes in this parameter, the β values are adjusted across a range of -7 to 7 and the impact on the swimming performance of a squirmer rod with $\varepsilon = 3$ at $Re = 0.01$ is investigated. The value of β considerably affects the swimming efficiency of the squirmer rod. This difference spans an order of magnitude (from 0.1 to 1). As mentioned in Subsection 4.2, the swimming efficiency of the pusher and the puller at a Re of 0.01 is close to each other, and as depicted in Fig. 10(a), the closer the value of β is to 0, the higher η is, while the higher the absolute value of β is, the lower η is. Therefore, η and β exhibit a relationship resembling a Gaussian distribution. Next, we examine the power expenditure (P) in Fig. 10(b). In contrast to the situation with η, the P values at $\beta = \pm 1$ are significantly lower than those at $\beta = \pm 7$. The drag power does not change with β due to the consistency in the steady speeds of squirmer rods with different swimming type factors at $Re = 0.01$. However, β as the ratio of B_2 to B_1 affects the surface self-propelled velocity distribution of the squirmer rod. Figure 11 shows the velocity vector distribution for $\beta = \pm 1$ and $\beta = \pm 5$. The smaller the absolute value of β, the more uniform the distribution of velocity, making it more similar to the neutral squirmer rod depicted in Fig. 3. In contrast, the larger the absolute value

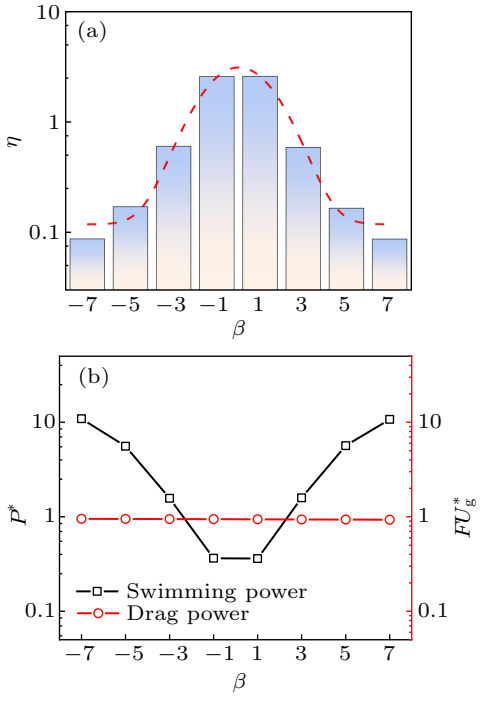


Fig. 10. Function of the swimming types (β) at $Re = 0.01$ for $\varepsilon = 3$. (a) Swimming efficiency and (b) power expenditure (P and FU_g are normalized by $B_1^2\mu/4$).

of β, the more the intensity of the self-propelled velocity at the heads and tails of both pushers and pullers is increased. Notably, the velocity directions at the two ends are opposite, which causes significant additional power expenditure during swimming as the enhancement of velocity at the head of the pusher and tail of the puller.

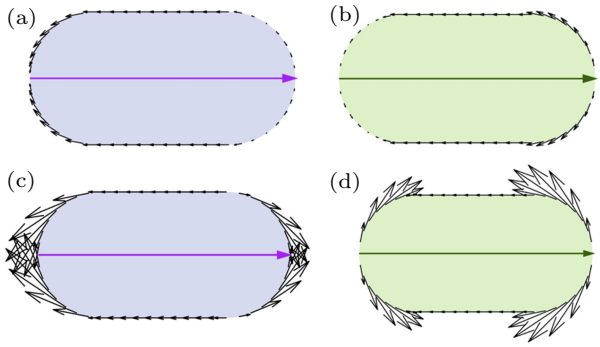


Fig. 11. Schematic diagram of the squirmer rod boundary tangential velocity vector for $\varepsilon = 3$, where the scale factor of the arrow corresponds to $\lambda = 0.8$. (a) $\beta = -1$, (b) $\beta = 1$, (c) $\beta = -5$, (d) $\beta = 5$.

Further analysis of the flow field in Fig. 12 reveals a significant observation. As the absolute value of β increases, the pressure gradient on the surface of the squirmer rod significantly intensifies. Specifically, for the pusher with $\beta = -5$, there is a notable increase in the difference in surface pressure, leading to more effective attraction of the surrounding fluid by the low-pressure areas on the sides of the microswimmer's body, while the high-pressure areas at the head and tail more forcefully expel the fluid. This phenomenon enhances the interaction between the microswimmer and fluid, thereby enlarging the recirculation zone around the head and providing the microswimmer with stronger propulsion. Conversely, when $\beta = -1$, the pressure difference on the surface of the pusher decreases, and its ability to attract and push the fluid weakens correspondingly, leading to a reduction in the recirculation zone around the head. Similarly, for pullers, when $\beta = 5$ compared to $\beta = 1$, the impact force on the fluid in the flow field becomes more intense, and the resistance encountered during motion also increases, with an expanded recirculation zone around the tail. Thus, as the absolute value of β increases, the hydrodynamic behavior of squirmer rods becomes more active in the fluid, potentially leading to increased energy consumption to maintain or achieve their desired swimming speed.

Therefore, although the swimming type ($\beta<0$ or $\beta > 0$) has a minimal impact on the swimming efficiency of the squirmer rod at low *Re* values, the closer the value of β is to 0, the lower the power expenditure and the higher the swimming efficiency we can achieve. Furthermore, the swimming efficiencies of $\beta = -1$ and $\beta = 1$ even exceed 1, indicating that compared to dragging a passive rod with an external force, the propulsion method of the squirmer rod is more energy-efficient (Fig. 10), suggesting that biomimetic self-propelled microswimmers, as a future development trend, may have advantages over microswimming devices driven by external fields in terms of energy savings.

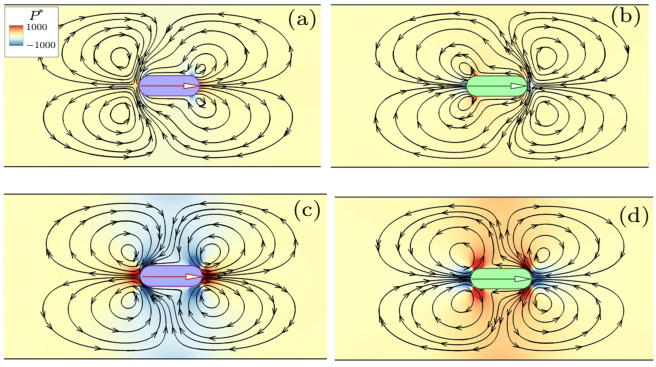


Fig. 12. Streamlines around a squirmer rod at $Re = 0.01$ for $\varepsilon = 3$. (a) $\beta = -1$, (b) $\beta = 1$, (c) $\beta = -5$, (d) $\beta = 5$.

4.4. Effects of the blockage ratios

Microswimmers do not always cruise in unrestricted flow field environments. Therefore, in this section, we explore the impact of the channel blockage ratio (κ) on the swimming efficiency and power expenditure of the squirmer rod, with *Re* set at 0.01. We demonstrated that the sign of the same β value has a minor impact on η and *P* of the squirmer rod at the low *Re* values above. For simplicity, we only present the results for the pusher ($\beta = -3$) depending on the blockage ratio (κ), including a comparison with the circular squirmer ($\varepsilon = 1$).

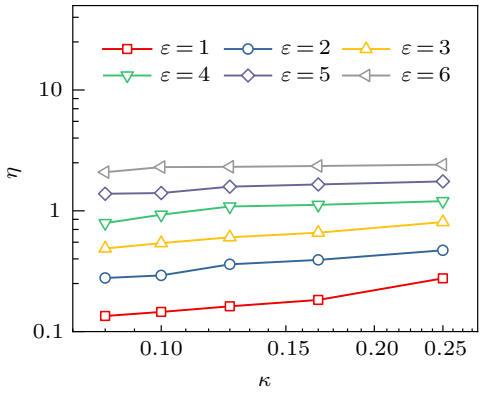


Fig. 13. Hydrodynamic efficiency as a function of the blockage ratios (κ) at $Re = 0.01$ for $\beta = -3$ and $\varepsilon = 1$–6.

The findings presented in Fig. 13 indicate that, without changing the diameter of the squirmer rod, as the blockage ratio κ increases, meaning the channel becomes narrower, both the circular squirmer and the squirmer rod exhibit an increase in η, which is unexpected. Typically, compression from the channel walls causes microswimmers within the channel to encounter greater resistance, as observed in our previous studies.[57] Using $\varepsilon = 2$ as a case in point, Fig. 14(a) illustrates that both FU_g and *P* increase as κ increases, and the degree of change in FU_g is greater. To reach the same velocity U_g during the channel compression, the passive rod requires a greater force to drag it forward. However, the squirmer rod achieves

efficient motion with relatively little energy loss due to its propulsion mechanism and interaction with the fluid, which explains why η of the squirmer rod improved.

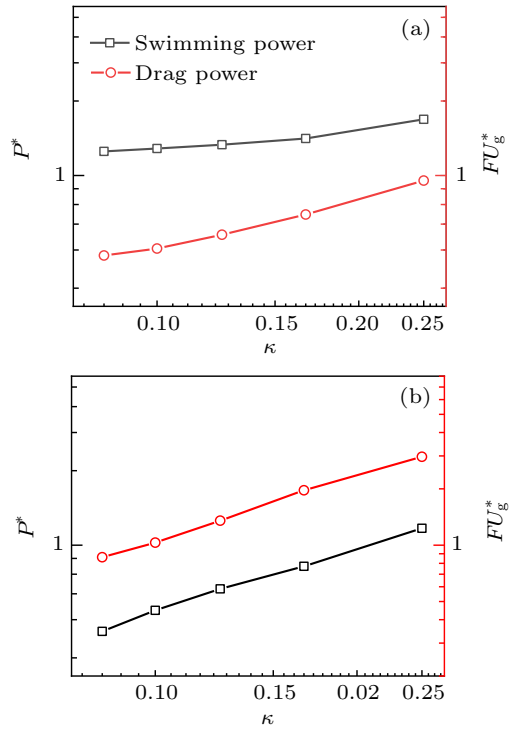


Fig. 14. Power expenditure as a function of the blockage ratios (κ) at $Re = 0.01$ for $\beta = -3$. (a) $\varepsilon = 2$ and (b) $\varepsilon = 6$. Note that (a) and (b) have the same range of coordinates.

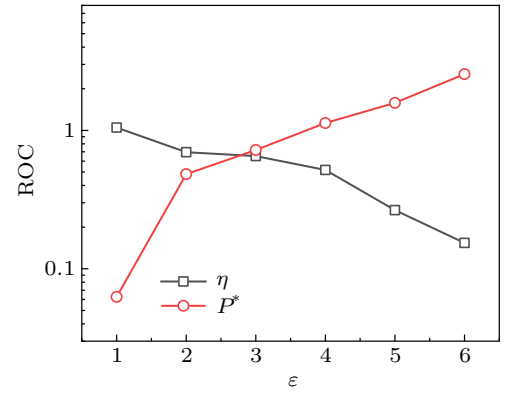


Fig. 15. Rate of change (ROC) in swimming power (P is normalized by $B_1^2\mu d/4$) and swimming efficiency with the aspect ratio of 1 to 6 for $\kappa$from 0.083 to 0.25.

Furthermore, we observe that the impact of κ on the swimming efficiency of squirmer rods with larger aspect ratios is less significant, and in some cases, almost negligible. As shown in Fig. 14(b), when $\varepsilon = 6$, both FU_g and P maintain the same variation trends. At this point, compared with externally driven propulsion, self-propelled microswimmers lose their advantage in terms of energy savings. In Fig. 15, for squirmer rods with varying aspect ratios, we present the rate of change (ROC) for η and power P across κ ranging from 0.083 to 0.25. As the channel narrows, the ROC of η for squirmer rods with larger aspect ratios becomes smaller, while the ROC for P increases. This result implies that in operational environments where the obstruction is intensified, enhancing the energy supply to longer squirmer rods does not significantly improve swimming efficiency. In contrast, opting for shorter squirmer rods is more cost-effective because a small increase in power consumption can significantly enhance swimming efficiency, especially for circular squirmers.

Next, we explore the streamline structures around the squirmer rods in the flow fields under different blockage ratios. Figures 16(a) and 16(c) specifically depict a pusher with $\varepsilon = 2$ swimming in channels with κ of 0.25 and 0.083, respectively. Under the effect of the pressure difference surrounding the body of the squirmer rod, the fluid has ample space to evolve in the wider channel, resulting in symmetrically large recirculation zones. However, as the channel narrows, the fluid is strongly influenced by the walls, leading to increased resistance and compression of circulation zones. Consequently, the squirmer rod is required to expand its energy to swim. Figures 16(b) and 16(d) show the case scenarios for $\varepsilon = 6$, which bear similarities to $\varepsilon = 2$ but with a critical difference. Due to the alteration in body length, the recirculation zones in narrower channels are positioned further from the center, tend to be closer to the ends of the head and tail, and the role of the pressure zones on the side of the body is much more pronounced, leading to a much greater increase in power expenditure compared to the $\varepsilon = 2$ case.

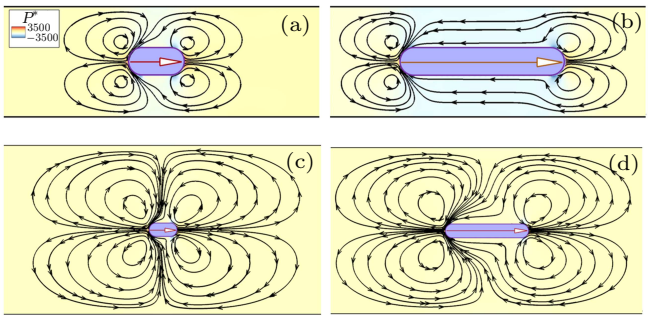


Fig. 16. Streamlines around a squirmer rod at $Re = 0.01$ for $\beta = 3$. (a) $\varepsilon = 2$, $\kappa = 0.25$, (b) $\varepsilon = 6$, $\kappa = 0.25$, (c) $\varepsilon = 2$, $\kappa = 0.083$ and (d) $\varepsilon = 6$, $\kappa = 0.083$.

In summary, in a more confined swimming environment, the squirmer rod compensates by increasing its energy consumption, a strategy that enables it to maintain or enhance its swimming efficiency despite increased resistance from the surrounding medium. This adaptive response to environmental constraints highlights the capability of the squirmer rod to optimize its propulsion mechanism under varying conditions, thereby achieving efficient locomotion even in restricted spaces.

5. Conclusion

This study employed the lattice Boltzmann method (LBM) to study the swimming efficiency of squirmer rods

numerically and based on the definition of η, we also analyzed the power expenditure changes of externally driven and self-propelled mechanisms — beneficial for designing and developing future microswimming devices. The swimming efficiency is significantly influenced by the aspect ratio (ε) and the squirmer-type factor (β) and is relatively insensitive to the Reynolds number (Re) and the blockage ratio (κ).

The analysis shows that at low Reynolds numbers, the values of P and η remain almost constant independent of Re and β. However, when the finite inertia is not negligible, pushers see an increase in η with rising Re, whereas pullers experience a decrease, positioning pushers as more efficient swimmers compared to pullers. Therefore, to enhance swimming efficiency without increasing power expenditure, selecting microswimmers with tail-driven propulsion mechanisms is an effective strategy. It is found that squirmer rods with a larger ε exhibit low P and high η. Longer squirmer rods achieve higher swimming speeds, akin to possessing more cilia for propulsion, whereas the elongation of the recirculation zones reduces resistance from the fluid, contributing to their superior swimming performance. In particular, values of P are similar for both modes of motion at $\varepsilon = 4$, and the power expenditure of the self-propulsion methods is less than that of the externally driven mechanisms when the aspect ratio increases further. Enhancing efficiency is potentially achieved by increasing the aspect ratio of the squirmer rod, and it has an advantage over the external field drive in saving energy. η and P are significantly influenced by the parameter β, and the closer β is to zero, the higher η and the lower P are. In contrast, the power expenditure of dragging a passive rod is little affected. Hence, the improvement in efficiency and reduction in energy consumption highlights the potential of fine-tuning the β value, especially in applications seeking efficient energy use. While η of the squirmer rod increases with κ, this improvement requires more power consumption. The larger the aspect ratio of the squirmer rod, the less significant the increase in η, with virtually no change observed for $\varepsilon = 6$. Therefore, in environments where channel constriction becomes more severe, smaller microswimmers offer a better cost-effectiveness ratio in terms of efficiency enhancement. This finding suggests that, in tightly confined spaces, optimizing the size and shape of microswimmers can lead to more efficient navigation strategies.

Appendix A: Validation of squirmer rods composed of circular squirmers

The effectiveness of the simulation of the squirmer model can be referred to in a previous work.[57] In Subsection 2.2, we proposed the formation of a squirmer rod, and it is necessary to verify whether the selection of the number of circular squirmers and the selection of the spacing between two neighboring circular squirmers can lead to the ideal model of the squirmer rod. As illustrated in Fig. A1, where both sides of the body are smooth. For an ideal squirmer rod composed of circular squirmer models, after being endowed with self-propelled velocity, the velocity of each point on both sides of the body is $-B_1$ (at this point $\theta = 90^\circ$ and -90°). Through integral calculations, we obtain the formula for the overall velocity of the ideal squirmer rod (the sum of the velocities in the y-direction is zero) — related to the aspect ratio ε and is described as follows:

$$U_{\rm s} = \frac{\int_0^{2\pi} u_x^{\rm s} r \,{\rm d}\theta - 4B_1(\varepsilon-1)r}{2\pi r + 4(\varepsilon-1)r} = -\left(1 - \frac{\pi}{2\pi + 4(\varepsilon-1)}\right)B_1, \tag{A1}$$

where $u_x^{\rm s}$ is the horizontal component of tangential velocity, r is the radius of the circle and ε is the aspect ratio. Notably, $U_{\rm s}$ represents the given speed rather than the steady speed U achieved after swimming. Comparing the self-propelled velocities of the squirmer rod model calculated using the LBM with the velocity values $U_{\rm s}$ of the ideal squirmer rod model, the velocity assignments for all three swimming types and squirmer rod models with aspect ratios ranging from 1 to 6 are in accordance with the theoretical values (Fig. A2), thus proving that the selection of the number of circular squirmers and their spacing is rational.

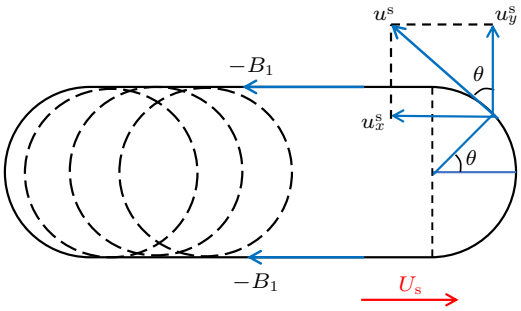


Fig. A1. Schematic diagram of a squirmer rod composed of circular squirmers. Note that the intersecting part of the circles is removed.

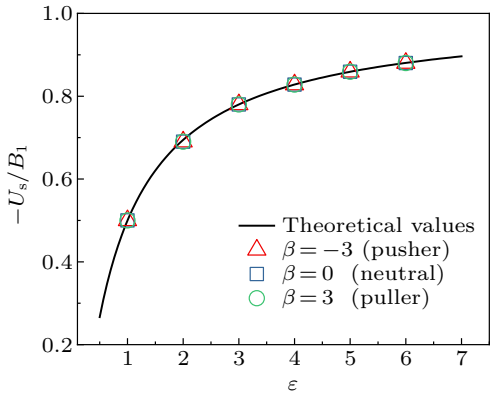


Fig. A2. Velocity assigned to a squirmer rod of different aspect ratios assembled by circular squirmers using the LBM compared to the theoretical values.

In addition, the free motion of a single squirmer rod in an unconfined area was simulated to validate the accuracy of the

LBM simulation of the squirmer model. In a square area with periodic boundary conditions in all directions, a squirmer rod with a diameter d of $40\Delta x$ and an aspect ratio of 3 is allowed to start from rest and move freely from the center of the area, with the *Re* set at 0.005. Although there is no theoretical solution for the squirmer rod model, it can be observed in Fig. A3 that the steady swimming speeds of all three types of squirmer rods can reach the same value at low *Re* values, which is similar to the results exhibited by the circular squirmer under the corresponding conditions, and demonstrates the reasonableness of the simulation of the squirmer rod in this study.

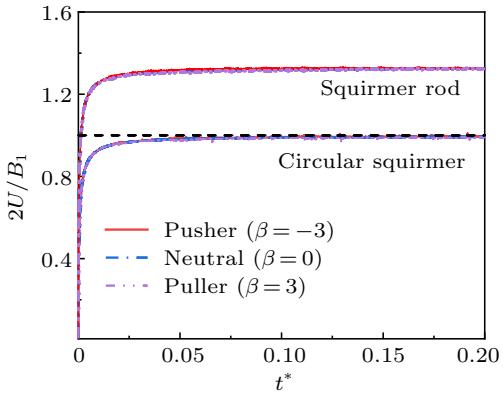


Fig. A3. Time history of free swimming to reach the normalized velocity $(2U/B_1)$ for different swimming types of squirmer rods and circular squirmers in a $20d \times 20d$ square at $Re = 0.005$. The time t is normalized by $t^* = tU/d$.

Acknowledgements

Project supported by the National Natural Science Foundation of China (Grant Nos. 12372251 and 12132015) and the Fundamental Research Funds for the Provincial Universities of Zhejiang (Grant No. 2023YW69).

References

[1] Ullrich F, Bergeles C, Pokki J, Ergeneman O, Erni S, Chatzipirpiridis G, Pané S, Framme C and Bradley J N 2013 *Invest. Ophthalmol. Vis. Sci.* **54** 2853
[2] Agrahari V, Agrahari V, Chou M L, Chew C H, Noll J and Burnouf T 2020 *Biomaterials* **260** 120163
[3] Wei X, Beltrán-Gastélum M, Karshalev E, de Ávila B E F, Zhou J, Ran D, Angsantikul, Fang R H, Wang J and Zhang L 2019 *Nano Lett.* **19** 1914
[4] Wu Z, Li J, de Ávila B E F, Li T, Gao W, He Q, Zhang L and Wang J 2015 *Adv. Funct. Mater.* **25** 7497
[5] Shintake J, Cacucciolo V, Shea H and Floreano D 2018 *Soft Robot.* **5** 466
[6] Ren Z, Hu W, Dong X and Sitti M 2019 *Nat. Commun.* **10** 2703
[7] Huang C, Lv J, Tian X, Wang Y, Yu Y and Liu J 2015 *Sci. Rep.* **5** 17414
[8] Qiu F and Nelson B J 2015 *Eng.* **1** 021
[9] Gong D, Cai J, Celi N, Feng L, Jiang Y and Zhang D 2018 *J. Magn. Magn. Mater.* **468** 148
[10] Darmawan B A, Lee S B, Go G, Nguyen K T, Lee H S, Nan M, Hong A, Kim C S, Li H, Bang D, Park J and Choi E 2020 *Sens. Actuators B Chem.* **324** 128752
[11] Akolpoglu M B, Dogan N O, Bozuyuk U, Ceylan H, Kizilel S and Sitti M 2020 *Adv. Sci.* **7** 2001256
[12] Alapan Y, Yasa O, Schauer O, Giltinan J, Tabak A F, Sourjik V and Sitti M 2018 *Sci. Robot.* **3** eaar4423
[13] Magdanz V, Khalil I S M, Simmchen J, Furtado G P, Mohanty S, Gebauer J, Xu H, Klingner A, Aziz A, Medina-Sánchez M, Schmidt O G and Misra S 2020 *Sci. Adv.* **6** eaba5855
[14] Blake J R 1971 *Bull. Aust. Math. Soc.* **5** 255
[15] Pedley T J 2016 *IMA J. Appl. Math.* **81** 488
[16] Magar V, Goto T and Pedley T J 2003 *Q. J. Mech. Appl. Math.* **56** 65
[17] Magar V and Pedley T J 2005 *J. Fluid Mech.* **539** 93
[18] Nie D, Ying Y, Guan G, Lin J and Ouyang Z 2023 *J. Fluid Mech.* **960** A31
[19] Ishikawa T, Locsei J T and Pedley T J 2008 *J. Fluid Mech.* **615** 401
[20] Ying Y, Jiang T, Nie D and Lin J 2022 *Phys. Fluids* **34** 013010
[21] Fadda F, Molina J J and Yamamoto R 2020 *Phys. Rev. E* **101** 052608
[22] Rühle F and Stark H 2020 *Eur. Phys. J. E* **43** 1
[23] Zheng K, Wang J, Zhang P and Nie D 2023 *AIP Adv.* **13** 025304
[24] Li G J and Ardekani A M 2014 *Phys. Rev. E* **90** 013010
[25] Lucarini G, Palagi S, Beccai L and Menciassi A 2014 *Int. J. Adv. Robot. Syst.* **11** 116
[26] Acemoglu A and Yesilyurt S 2014 *Biophys. J.* **106** 1537
[27] Ullrich F, Qiu F, Pokki J, Huang T, Pané S and Nelson B J 2016 *IEEE International Conference on Biomedical Robotics and Biomechatronics (BioRob)*, June 26–29, 2016 Singapore, p. 470
[28] Ghanbari A and Bahrami M 2011 *J. Intell. Robot. Syst.* **63** 399
[29] Omori T, Ito H and Ishikawa T 2020 *Proc. Natl. Acad. Sci. USA* **117** 30201
[30] Ouyang Z, Lin J and Ku X 2018 *Phys. Fluids* **30** 085304
[31] Leshansky A M, Kenneth O, Gat O and Avron J E 2007 *New J. Phys.* **9** 145
[32] Michelin S and Lauga E 2010 *Phys. Fluids* **22** 011401
[33] Chisholm N G, Legendre D, Lauga E and Khair A S 2016 *J. Fluid Mech.* **796** 233
[34] Eastham P S and Shoele K 2020 *Phys. Rev. Fluids* **5** 063102
[35] Binagia J P, Phoa A, Housiadas K D and Shaqfeh E S G 2020 *J. Fluid Mech.* **900** A4
[36] Wang S and Ardekani A 2012 *Phys. Fluids* **24** 013010
[37] Zhu L, Lauga E and Brandt L 2013 *J. Fluid Mech.* **726** 285
[38] Ouyang Z, Lin Z, Lin J, Yu Z and Phan-Thien N 2023 *J. Fluid Mech.* **959** A25
[39] Sahari A, Headen D and Behkam B 2012 *Biomed. Microdevices* **14** 999
[40] Merkel T J, Jones S W, Herlihy K P, Kersey F R, Shields A R, Napier M, Luft J C, Wu H, Zamboni W C, Wang A Z, Bear J E and DeSimone J M 2011 *Proc. Natl. Acad. Sci. USA* **108** 586
[41] Nejati S, Vadeghani E M, Khorshidi S and Karkhaneh A 2020 *Eur. Polym. J.* **122** 109353
[42] Christian D A, Cai S, Garbuzenko O B, Harada T, Zajac A L, Minko T and Discher D E 2009 *Mol. Pharmaceutics* **6** 1343
[43] Ying Y, Jiang T, Li S, Nie D and Lin J 2024 *Phys. Scr.* **99** 025304
[44] Zantop A W and Stark H 2020 *Soft Matter* **16** 6400
[45] Ouyang Z and Lin J 2021 *Phys. Fluids* **33** 073102
[46] Ishikawa T 2019 *Micromachines* **10** 33
[47] Biondi S A, Quinn J A and Goldfine H 1998 *AIChE J.* **44** 1923
[48] Zhang J, Liu K and Ding Y 2022 *Chin. Phys. B* **31** 14702
[49] He X and Luo L S 1997 *Phys. Rev. E* **56** 6811
[50] Wolf-Gladrow D A 2004*Lattice-Gas Cellular Automata and Lattice Boltzmann Models: An Introduction* (1st edn.) (Berlin: Springer) p. 9
[51] Qian Y H, d'Humières D and Lallemand P 1992 *Europhys. Lett.* **17** 479
[52] Chapman S and Cowling T G 1970 *Math. The Mathematical Theory of Non-Uniform Gases* (3rd edn.) (Cambridge: Cambridge University Press) p. 119
[53] Lallemand P and Luo L S 2003 *J. Comput. Phys.* **184** 406
[54] Mei R, Yu D, Shyy W and Luo L S 2002 *Phys. Rev. E* **65** 041203
[55] Aidun C K, Lu Y and Ding E J 1998 *J. Fluid Mech.* **373** 287
[56] Michelin S and Lauga E 2010 *Phys. Fluids* **22** 113901
[57] Li S, Ying Y and Nie D 2023 *Fluid Dyn. Res.* **55** 055504